Supplementary Information for: Site-specific electronic and magnetic excitations of the skyrmion material Cu_2OSeO_3

Yanhong Gu,[1] Yilin Wang,[2,*] Jiaqi Lin,[2,†] Jonathan Pelliciari,[1] Jiemin Li,[1] Myung-Geun Han,[2] Marcus Peter Schmidt,[3] Gabriel Kotliar,[2,4] Claudio Mazzoli,[1] Mark P. M. Dean,[2] and Valentina Bisogni[1,‡]

[1] *National Synchrotron Light Source II, Brookhaven National Laboratory, Upton, NY 11973, USA.*

[2] *Department of Condensed Matter Physics and Materials Science, Brookhaven National Laboratory, Upton, New York 11973, USA.*

[3] *Max Planck Institute for Chemical Physics of Solids, Nöthnitzer Straße 40, D-01187 Dresden, Germany.*

[4] *Department of Physics and Astronomy, Rutgers University, Piscataway, New Jersey 08856, USA.*

* Present address: Hefei National Laboratory for Physical Sciences at Microscale, University of Science and Technology of China, Hefei, Anhui 230026, China.

† Present address: Department of Physics, Westlake University, Hangzhou, China.

‡ bisogni@bnl.gov

Supplementary Note 1: Density Functional Theory Calculations

We performed density functional theory (DFT) combined with Wannier90 calculations to estimate the crystal field splitting. The DFT part of the calculation has been done by the Vienna Ab-initio Simulation Package (VASP)[1] with projector augmented-wave (PAW) pseudopotential[2,3] and Perdew-Burke-Ernzerhof parametrization of the generalized gradient approximation (GGA-PBE) exchange-correlation functionals[4]. The energy cutoff of the plane-wave basis is set to be 500 eV, and a Γ-centered $11 \times 11 \times 11$ K-point grid was used.

The $3d$ orbitals are defined with respect to local cartesian-coordinates shown in Supplementary Figure 1, as well as in Fig. 2**b** of the main text. The local z-axes are chosen to be along the local 3-fold rotational axis for the Cu-I sites and normal to the CuO_4 plane for the Cu-II sites, respectively. As a result of the crystallization environment, Cu-I with an approximately trigonal bipyramidal coordination, has a formal C_3 site symmetry. Cu-II instead has an approximately square pyramidal surrounding and a formal C_1 site symmetry, i.e. no symmetry.

A tight binding (TB) Hamiltonian consisting of $3d$ orbitals from four Cu-I sites and twelve Cu-II sites is then obtained by the maximally localized Wannier functions method[5,6]. The

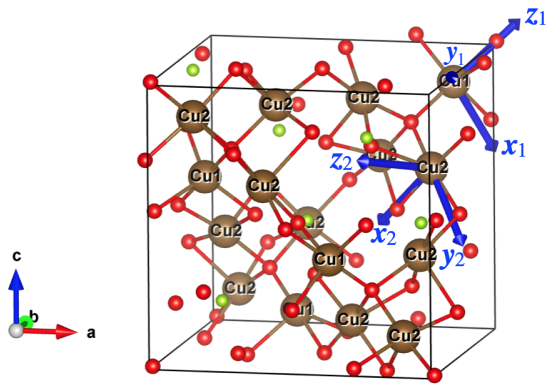

Supplementary Figure 1. The local coordindates (blue arrows) with respect to which the Wannier functions are defined. The local z-axis are chosen to be along the local 3-fold rotational axis for the Cu-I sites (z_1) and normal to the CuO_4 plane for the Cu-II sites (z_2), respectively.

local on-site crystal field Hamiltonian for the Cu-I and Cu-II sites are (energy in eV):

$$\hat{H}^{\text{CF}}_{\text{Cu-I}} = \begin{array}{c} \\ d_{z^2} \\ d_{xz} \\ d_{yz} \\ d_{x^2-y^2} \\ d_{xy} \end{array} \begin{array}{c} \begin{array}{ccccc} d_{z^2} & d_{xz} & d_{yz} & d_{x^2-y^2} & d_{xy} \end{array} \\ \begin{pmatrix} -0.001 & 0 & 0 & 0 & 0 \\ 0 & -1.313 & 0 & 0.120 & 0 \\ 0 & 0 & -1.313 & 0 & -0.120 \\ 0 & 0.120 & 0 & -1.178 & 0 \\ 0 & 0 & -0.120 & 0 & -1.178 \end{pmatrix} \end{array}, \tag{S1}$$

$$\hat{H}^{\text{CF}}_{\text{Cu-II}} = \begin{array}{c} \\ d_{z^2} \\ d_{xz} \\ d_{yz} \\ d_{x^2-y^2} \\ d_{xy} \end{array} \begin{array}{c} \begin{array}{ccccc} d_{z^2} & d_{xz} & d_{yz} & d_{x^2-y^2} & d_{xy} \end{array} \\ \begin{pmatrix} -1.077 & -0.009 & -0.112 & 0.017 & -0.020 \\ -0.009 & -1.243 & 0.035 & -0.026 & 0.043 \\ -0.112 & 0.035 & -1.364 & -0.014 & -0.011 \\ 0.017 & -0.026 & -0.014 & 0.282 & 0.258 \\ -0.020 & 0.043 & -0.011 & 0.258 & -1.077 \end{pmatrix} \end{array}. \tag{S2}$$

Overall, the energy levels displayed in the above local crystal field Hamiltonians are slightly adjusted with respect to the original DFT energy levels, in order to obtain a reasonable set of parameters for initializing the fitting of the experimental RIXS results. This adjustment is necessary because the DFT calculations are not very accurate for the $3d$ transition metal oxides. This statement can be better understood referring to Supplementary Figure 2**a** (**b**), that displays the RIXS spectrum measured before (after) the Cu L_3 edge as being mostly sensitive to Cu-I (Cu-II) site, respectively. The raw DFT levels, overlaid to the experimental data as grey dashed lines, clearly underestimate the crystal field energies for both Cu-I and Cu-II by as much as ~ 0.45 eV. Rather, the corrected DFT levels displayed as blue dashed lines in the same figure match well the experimental data. To be specific, the corrected DFT levels have been obtained by shifting for Cu-I the orbitals $d_{x^2-y^2}$ and d_{xy} down by 0.4 eV; while for Cu-II the orbital d_{z^2} down by 0.12 eV, the orbital $d_{x^2-y^2}$ up by 0.25 eV and the orbital d_{xy} up by 0.45 eV.

Since for C_3 site symmetry the five $3d$ orbitals split into one A_{1g} representation (d_{z^2}) and two coinciding E_g representations [(d_{xz}, d_{yz}) and ($d_{x^2-y^2}$, d_{xy})], the resulting $\hat{H}^{\text{CF}}_{\text{Cu-I}}$ in Supplementary Equation S1 is unavoidably a mix between the two E_g representations, i.e.

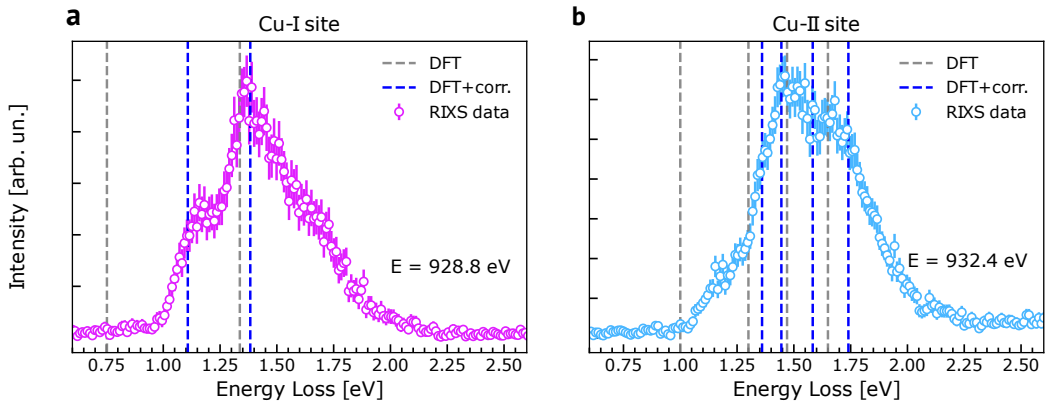

Supplementary Figure 2. density functional theory (DFT) levels for Cu-I site (**a**) and Cu-II site (**b**): raw DFT levels are displayed as grey dashed lines, while the corrected DFT levels resulting from Supplementary Equations S1-S2 are displayed as blue dashed lines. The calculated levels are overlaid to the RIXS spectra measured at E=928.8 eV (932.4 eV), mostly sensitive to Cu-I (Cu-II), respectively.

d_{xz} mixes with $d_{x^2-y^2}$ and d_{yz} mixes with d_{xy}. Due to the lack of symmetry for Cu-II site, the terms in $\hat{H}^{\mathrm{CF}}_{\text{Cu-II}}$ result completely mixed.

Diagonalizing $\hat{H}^{\mathrm{CF}}_{\text{Cu-I}}$ and $\hat{H}^{\mathrm{CF}}_{\text{Cu-II}}$ yields new wavefunctions with the expected mixed orbital characters, as displayed in Supplementary Table 1 for Cu-I and in Supplementary Table 2 for Cu-II. For simplicity, we label the new wavefunctions as d_{z^2}, d_{xz}, d_{yz}, $d_{x^2-y^2}$, d_{xy} by simply referring to their dominant orbital component (above 80%), higlighted in blue in Supplementary Tables 1-2. For example, for Cu-I, the first wavefunction Wf1 = -0.863d_{xz}+0.505$d_{x^2-y^2}$ is referred to as d_{xz}.

The eigenvalues of the diagonalized $\hat{H}^{\mathrm{CF}}_{\text{Cu-I}}$ and $\hat{H}^{\mathrm{CF}}_{\text{Cu-II}}$ provide the energy of the crystal field levels for Cu-I and Cu-II sites, respectively. These values are summarized in Supplementary Table 3, second and fifth columns, and are labelled by their dominant orbital character. The Cu-I topmost hole orbital energy (ground state, GS) is of reference energy and set to 0 eV. The GS level of the Cu-II sites is higher in energy than Cu-I by about 0.33 eV, so the Cu-II sites resonate at higher energy than the Cu-I sites.

Furthermore, for each Cu species, the energy difference between the ground state level with respect to each crystal field level is calculated in the third and sixth columns of Supplementary Table 3, respectively for Cu-I and Cu-II. Such values provide a good match with

the *dd*-excitation energies extracted from the experiment, see Supplementary Table 4, and discussed in the main text.

	Wf1 [-1.383 eV]	Wf2 [-1.383 eV]	Wf3 [-1.108 eV]	Wf4 [-1.108 eV]	Wf5 [0 eV]
d_{z^2}	0	0	0	0	1
d_{xz}	-0.863	0	0.505	0	0
d_{yz}	0	-0.863	0	-0.505	0
$d_{x^2-y^2}$	0.505	0	0.863	0	0
d_{xy}	0	-0.505	0	0.863	0

Supplementary Table 1. Orbital components of the Cu-I wavefunctions after diagonalization of $\hat{H}^{\mathrm{CF}}_{\text{Cu-I}}$. The wavefunctions are progressively labelled as Wf1 to Wf5, in order of increasing eigenvalues.

	Wf1 [-1.410 eV]	Wf2 [-1.253 eV]	Wf3 [-1.115 eV]	Wf4 [-1.030 eV]	Wf5 [0.330 eV]
d_{z^2}	0.311	-0.123	-0.269	0.903	-0.009
d_{xz}	-0.196	-0.927	-0.287	-0.144	0.012
d_{yz}	0.926	-0.182	0.113	-0.310	0.010
$d_{x^2-y^2}$	-0.012	-0.066	0.165	0.034	-0.984
d_{xy}	0.084	0.298	-0.898	-0.257	-0.180

Supplementary Table 2. Orbital components of the Cu-II wavefunctions after diagonalization of $\hat{H}^{\mathrm{CF}}_{\text{Cu-II}}$. The wavefunctions are progressively labelled as Wf1 to Wf5, in order of increasing eigenvalues.

Supplementary Note 2: X-ray Absorption Spectroscopy (XAS) and Resonant Inelastic X-ray Scattering (RIXS) simulations at Cu-L_3 edge

Using the crystal-field energies and the orbital characters identified within the above DFT section, we simulate the XAS and RIXS spectra based on single-atom model using the EDRIXS code[7], by accounting for all the differently oriented Cu ions within the unit cell.

Cu-I			**Cu-II**		
Orbital	Energy [eV]	*dd*-exc [eV]	Orbital	Energy [eV]	*dd*-exc [eV]
d_{z^2} (GS)	0	0	$d_{x^2-y^2}$ (GS)	0.330	0
d_{xy}	-1.108	1.108	d_{z^2}	-1.030	1.360
$d_{x^2-y^2}$	-1.108	1.108	d_{xy}	-1.115	1.445
d_{xz}	-1.383	1.383	d_{xz}	-1.253	1.583
d_{yz}	-1.383	1.383	d_{yz}	-1.410	1.740

Supplementary Table 3. Energy of the Cu-I and Cu-II calculated crystal-field levels and corresponding *dd*-excitation energies.

For the current case with only one hole per site, the spectra are not sensitive to the exact Slater parameters, so standard values and rescaling were used here[8].

The selected geometrical configuration reproduces the experimental conditions. In particular, the scattering plane contains the [001] and [110] directions. X-rays with π-polarization are incident at 20° with respect to the [001] direction and the sum of the π and σ polarized x-rays scattered around 90° are analyzed. Moreover, the life times of intermediate and final states are 0.6 eV and 0.2 eV, respectively.

Supplementary Figure 3**a** (3**b**) are the calculated RIXS map of the four Cu-I [twelve Cu-II] sites. There are two excitations, E1 and E3, for the Cu-I sites; and four excitations, E2, E4, E5, E6, for the Cu-II sites. The resonant energies for Cu-I and Cu-II are both offset by the same value, $\sim$ 931 eV, to match the experimental finding. For each RIXS map, we perform the integral over the energy loss axis in order to obtain the corresponding absorption spectrum associated with each Cu site (see solid line in slate-blue color). The offset between the absorption maxima is determined by the energy difference between the Cu-I and Cu-II ground state levels. By performing instead the integral over the photon energy axis, we obtain the fundamental RIXS spectrum for each individual Cu site (see solid line in purple color). The fundamental RIXS spectrum provides information on the *dd*-excitations cross-section for each site. These ratios are then used for the analysis of the experimental data. The sum of the Cu-I and Cu-II RIXS map represents the total RIXS map [see Supplementary Figure 3**c**], which can be compared with the experimental data shown in Fig. 1**c** of the

main text. Supplementary Figure 3**d** instead reproduces the individual absorption spectra obtained for each Cu sites and their sum, which provides the total absorption spectrum in the approximation of no interference.

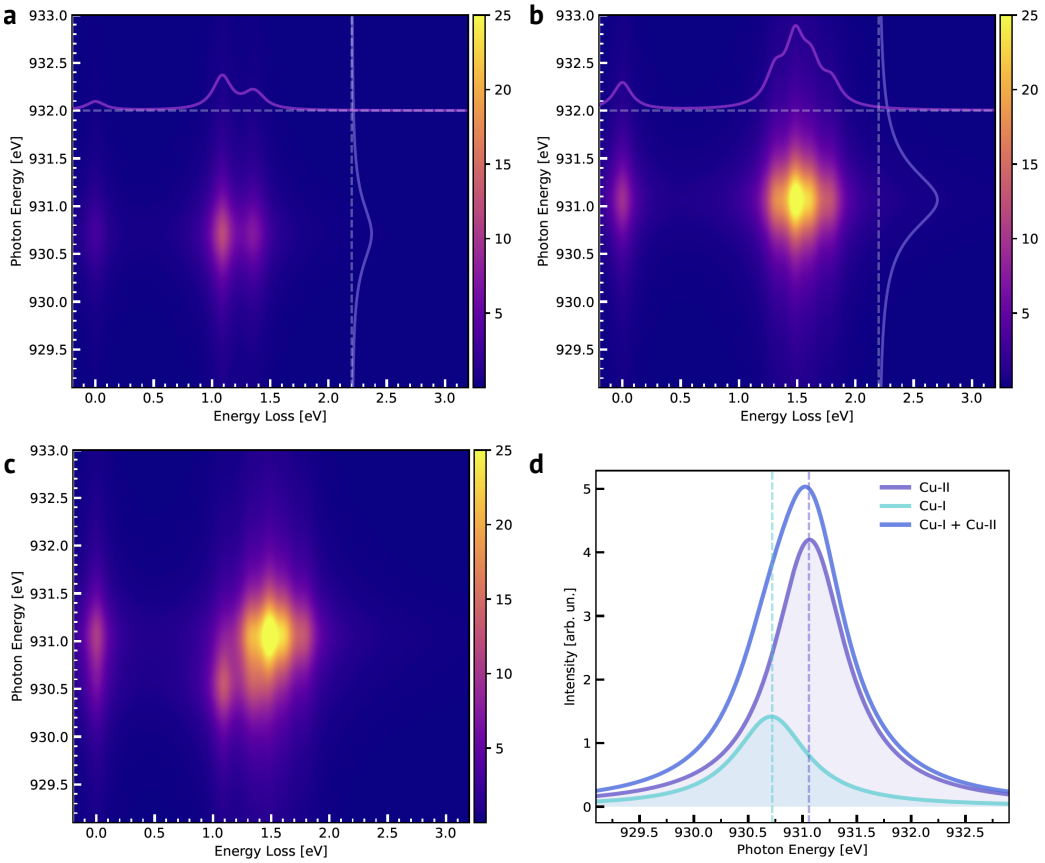

Supplementary Figure 3. Calculated Resonant Inelastic X-ray Scattering (RIXS) map of **a** the four Cu-I sites and **b** the twelve Cu-II sites. **c** The total RIXS map, contributed from the Cu-I and Cu-II sites. **d** The integrated RIXS intensities as a function of the incident photon energy, as extracted from the calculated site responses and their sum.

Supplementary Note 3: Fitting of the RIXS data to disentangle the site-dependent *dd*-excitations

The Cu L_3 RIXS spectrum of Cu_2OSeO_3 is dominated by crystal-field *dd*-excitations in the 1-2 eV energy range (see Fig. 2**a** of the main text). The energy-proximity of the two Cu species present in this material means that a theory-constrained fit analysis is required.

By using the DFT energies for the *dd*-excitations in Supplementary Table 3, and the RIXS intensity obtained from the single-atom model calculations, we can simulate the fundamental RIXS spectra associated with each Cu species, as displayed in Fig. 2**c** for Cu-I and in Fig. 2**d** for Cu-II by using equal-width Gaussian profiles for each *dd* excitation peak. These fundamental spectra allow to extract the following intensity ratios: $I_{E1} : I_{E3} = 1 : 1.23$ for Cu-I and $I_{E2} : I_{E4} : I_{E5} : I_{E6} = 1 : 1.62 : 1.16 : 1.05$ for Cu-II, where the lowest-energy *dd*-excitation intensity for each Cu species is taken as a reference. These ratios are useful for fitting the data, when different widths for the *dd*-excitations could be used.

Next, we fit the RIXS spectra displayed in Fig. 2**a**. By using a normalized Gaussian profile for each *dd*-excitation, we build the following fitting model:

$$I_{\mathrm{RIXS}}^{\mathrm{total}} = I_{\mathrm{RIXS}}^{\mathrm{CuI}} + I_{\mathrm{RIXS}}^{\mathrm{CuII}} \tag{S3}$$

where,

$$I_{\mathrm{RIXS}}^{\mathrm{CuI}} = A^{\mathrm{CuI}} \cdot (G_1 + 1.23 \cdot G_3) \tag{S4}$$

$$I_{\mathrm{RIXS}}^{\mathrm{CuII}} = A^{\mathrm{CuII}} \cdot (G_2 + 1.62 \cdot G_4 + 1.16 \cdot G_5 + 1.05 \cdot G_6) \tag{S5}$$

with G_1-G_6 being area-normalized Gaussian functions, and $A^{\mathrm{CuI}}/A^{\mathrm{CuII}}$ being amplitude factors for Cu-I/Cu-II site, respectively. In reference to the area-normalized RIXS spectra mentioned in the main text, $(G_1 + 1.23 \cdot G_3) = \tilde{I}_{RIXS}^{\mathrm{CuI}}$, with a total area of 2.23, while $(G_2 + 1.62 \cdot G_4 + 1.16 \cdot G_5 + 1.05 \cdot G_6) = \tilde{I}_{RIXS}^{\mathrm{CuII}}$, with a total area of 4.83.

To perform the fitting of the RIXS spectra versus incident energy, we leave the amplitude parameters $A^{\mathrm{CuI}}/A^{\mathrm{CuII}}$ completely free, as well as the width of the Gaussian profiles. Instead, we constrain: *i*) the Gaussian centers within $\pm$ 175 meV from the DFT *dd*-excitation energies reported in Supplementary Table 3; *ii*) the *dd*-excitations intensity ratio to the single-ion calculated values as set in the fitting model.

The fitted spectra are presented in Fig. 3**a-p**, where each panel refers to a specific incident energy and displays the raw data (circular markers), the fitted Gaussian components G_1 to G_6 (solid filling) and their sum (solid line).

The first main result of the fitting is the center position of the G_1 - G_6 components, reported in Fig. 3**q-r**. The values display very small variation as a function of incident

energy, indicating that the fitting model is pretty adequate. Their average and error (as standard deviation versus the values obtained for each incident energy) are summarized in Supplementary Table 4. Furthermore, the averaged energies are reasonably close to the calculated values (see Supplementary Table 3). The maximum deviation between the experimental and calculated values is $\sim$ 120 meV, well below the $\pm$ 175 meV value set in the fitting constraint, confirming that this choice is appropriate.

The averaged full width half maximum (FWHM) of the fitted Gaussians as a function of incident energy is presented in the fourth column of Supplementary Table 4, together with the respective error (again, considered as standard deviation).

Site	**Excitation**	**Exp. Energy [eV]**	**Exp. FWHM [eV]**
Cu-I	E1	1.18 $\pm$ 0.015	0.19 $\pm$ 0.01
	E3	1.40 $\pm$ 0.010	0.21 $\pm$ 0.012
Cu-II	E2	1.40 $\pm$ 0.010	0.21 $\pm$ 0.012
	E4	1.57 $\pm$ 0.010	0.26 $\pm$ 0.017
	E5	1.67 $\pm$ 0.012	0.27 $\pm$ 0.018
	E6	1.86 $\pm$ 0.014	0.31 $\pm$ 0.020

Supplementary Table 4. Fit results averaged over for all the Resonant Inelastic X-ray Scattering (RIXS) spectra measured across the Cu L_3 edge: the first column reports the label assigned to the *dd*-excitations according to Fig. 2**b**; the second columns displays the center values for the *dd*-excitations; and the third column displays the full width half maximum values.

Finally, we can note that the FWHM of the *dd*-excitations systematically increases with the increasing of the *dd*-excitation energy itself: this can be explained with a shortening of the lifetime associated with the higher-energy of the excitations.

Supplementary References

1. Kresse, G. & Furthmüller, J. Efficient iterative schemes for ab initio total-energy calculations using a plane-wave basis set. *Phys. Rev. B* **54**, 11169 (1996).
2. Blöchl, P. E. Projector augmented-wave method. *Physical Review B* **50**, 17953 (1994).
3. Kresse, G. & Joubert, D. From ultrasoft pseudopotentials to the projector augmented-wave method. *Physical Review B* **59**, 1758 (1999).

4. Perdew, J. P., Burke, K. & Ernzerhof, M. Generalized Gradient Approximation Made Simple. *Physical Review Letters* **77**, 3865 (1996).

5. Marzari, N., Mostofi, A. A., Yates, J. R., Souza, I. & Vanderbilt, D. Maximally localized Wannier functions: Theory and applications. *Reviews of Modern Physics* **84**, 1419 (2012).

6. Mostofi, A. A. *et al.* wannier90: A tool for obtaining maximally-localised Wannier functions. *Computer Physics Communications* **178**, 685–699 (2008).

7. Wang, Y. L., Fabbris, G., Dean, M. P. M. & Kotliar, G. EDRIXS: An open source toolkit for simulating spectra of resonant inelastic x-ray scattering. *Computer Physics Communications* **243**, 151–165 (2019).

8. Cowan, R. D. *The Theory of Atomic Structure and Spectra* (University of California Press, 1981).